Nanoscale Motion of Soft Nanoparticles in Unentangled and Entangled Polymer Matrices

M. Lungova,[1,*] M. Krutyeva,[1] W. Pyckhout-Hintzen,[1] A. Wischnewski,[1] M. Monkenbusch,[1] J. Allgaier,[1] M. Ohl,[1] M. Sharp,[2] and D. Richter[1]

[1]*Jülich Centre for Neutron Science (JCNS) & Institute for Complex Systems (ICS), Forschungszentrum Jülich GmbH, 52425 Jülich, Germany*

[2]*Institute Laue Langevin (ILL), 38000 Grenoble, France and European Spallation Source (ESS), 22363 Lund, Sweden*

(Received 28 April 2016; published 28 September 2016)

We have studied the motion of polyhedral oligomeric silsesquioxane (POSS) nanoparticles modified with poly(ethylene glycol) (PEG) arms immersed in PEG matrices of different molecular weight. Employing neutron spin echo spectroscopy in combination with pulsed field gradient (PFG) NMR we found the following. (i) For entangled matrices the center of mass mean square displacement (MSD) of the PEG-POSS particles is subdiffusive following a $t^{0.56}$ power law. (ii) The diffusion coefficient as well as the crossover to Fickian diffusion is independent of the matrix molecular weight and takes place as soon as the center of mass has moved a distance corresponding to the particle radius—this holds also for unentangled hosts. (iii) For the entangled matrices Rubinstein's scaling theory is validated; however, the numbers indicate that beyond Rouse friction the entanglement constraints appear to strongly increase the effective friction even on the nanoparticle length scale imposing a caveat on the interpretation of microrheological experiments. (iv) The oligomer decorated PEG-POSS particles exhibit the dynamics of a Gaussian star with an internal viscosity that rises with an increase of the host molecular weight.

DOI: 10.1103/PhysRevLett.117.147803

The scale-dependent viscoelastic properties of soft matter systems—in particular polymer melts and concentrated solutions—are reflected in the motion of small particles embedded in such systems [1]. This has been used in microrheology as a means of probing the local dynamics of complex fluids [2–4]. Already Brochard and de Gennes [5] pointed out that the scale-dependent viscosity in a polymer melt will severely influence the transport properties of small colloidal particles. The Stokes-Einstein relation loses its validity and instead a local, scale-dependent viscosity of the complex fluid comes into play.

In this context for polymer melts the reptation tube size is the crucial spacial scale discriminating the dynamics of nanoparticles with sizes smaller or larger than the tube diameter d_{tube}. Based on this scale-dependent polymer dynamics, Rubinstein *et al.* [6] developed a scaling theory for the diffusion of nonsticky nanoparticles (NP) in a polymer matrix with precise predictions for the different size-dependent motional regimes of the NP. In particular, for NP smaller than d_{tube}, a subdiffusive behavior with a mean square center of mass (c.m.) displacement (MSD) $\langle r^2_{\mathrm{c.m.}}(t)\rangle \propto t^{1/2}$ was predicted which crosses over to Fickian diffusion when the NP have moved distances corresponding to their size. NP larger than d_{tube} are heavily restricted in their motion. Experimentally nanoparticle motion on nanoscopic scales became accessible via x-ray photon correlation spectroscopy (XPCS) [7–10]. Nanoparticle motions in glassy polymer materials, melts, and solutions were investigated. Hyperdiffusive properties were found that were related to strain-induced motion in glasses or to hopping between cages formed by the entangled polymer chains in the melt [7]. Recently, concentrated polystyrene solutions, where nanoparticles of a "size" R always larger than the solution mesh size and in the order of the solution tube diameter were studied [8]. For all conditions, subdiffusive motion with $\langle r^2_{\mathrm{c.m.}}\rangle \propto t^{\alpha}$ with $\alpha \simeq 0.5$ was found even though the maximum MSD significantly exceeded the particle diameter.

In this Letter we present a neutron spin-echo (NSE) study of the translational diffusion and the internal dynamics of PEG-POSS (POSS=polyhederal oligomeric silsesquioxane) nanoparticles that were grafted with poly (ethylene glycol) (PEG) oligomers immersed in PEG polymer matrices of different molecular weight.

The PEG-POSS particles were purchased from Hybrid Plastics, USA, and purified by triple fractionation. The final product was chemically analyzed leading to an average functionality $f_{\mathrm{POSS}} = 7.5$ and a polymerization degree of $n_{\mathrm{arm}} = 11.7$, terminated with CH_3 end groups. As matrix polymers, deuterated PEG chains of three different molecular weights were synthesized using standard anionic ring opening polymerization techniques with potassium *tert*-butoxide as initiator. The polymers were characterized by ^{1}H-NMR to determine the molecular weights and by size exclusion chromatography with PEG calibration to determine the polydispersities. The polydispersity indices were $M_w/M_n = 1.02$ and the matrix M_w values were 1.7 (1.5), 21.6 (20), and 83.1 kg/mol (80 K), respectively.

All mixtures of the linear PEG chains with the PEG-POSS particles were dissolved in *tert*-butanol and subsequently freeze dried at $T = -5\,^{\circ}\mathrm{C}$ to ensure good dispersion. PEG-POSS in PEG are to be considered "nonsticky,"

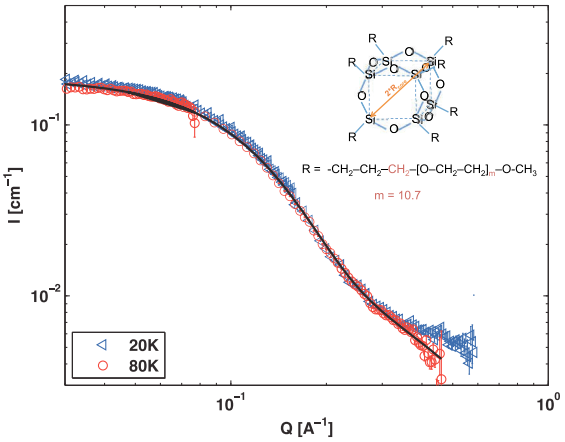

FIG. 1. SANS intensity of the PEG-POSS nanoparticles in PEG melts ($\phi_{\mathrm{PEG-POSS}} = 0.01$). The line is a fit to a micellar form factor (see text). The inset shows the chemical structure of the POSS core.

athermal nanoparticles without enthalpic interaction. All three samples investigated had a nanoparticle volume fraction $\phi_{\mathrm{PEG-POSS}} = 0.05$ (0.01 for SANS).

The PEG-POSS structure in the linear matrices was characterized by small-angle neutron scattering (SANS) experiments that were performed on the KWS-1 diffractometer at MLZ in Garching, Germany [11]. Neutron spin echo experiments were performed at the IN15 instrument at ILL Grenoble, France [12]. At a temperature of 400 K a time range from 0.1 to 250 ns was covered. Using the same samples, also pulsed field gradient (PFG) NMR experiments using a Bruker Minispec Analyzer *mq20* were performed at $T = 400$ K to measure the translational PEG-POSS diffusion coefficient on a micrometer scale.

Figure 1 displays background corrected SANS results from PEG-POSS particles at 1% solution in the 20 and 80 K deuterated matrices. As may be seen, the PEG-POSS form factors for both matrices are identical. The form factors were fitted using an RPA model including a micellar-like model by Pedersen *et al.* [13,14] for the PEG-POSS. The only fitting parameter was the statistical segment length $l_{\mathrm{st}}^{\mathrm{NP}}$ that came out to $l_{\mathrm{st}}^{\mathrm{NP}} \simeq 5.8 \pm 0.1$ Å, a value close to what would be expected for PEG chains ($l_{\mathrm{st}}^{\mathrm{matrix}} = 5.9$ Å [15]) in the melt. From a Guinier analysis the radius of gyration was determined to $R_g = 16.3 \pm 0.6$ Å leading to an effective PEG-POSS particle radius of 20.5 Å.

Figure 2 presents NSE spectra from the three samples (a) 1.5, (b) 20, and (c) 80 K for from above $Q = 0.07$, 0.09, 0.14 and 0.19 Å^{-1} with $Q = 4\pi/\lambda \sin(\theta/2)$, where λ is the neutron wavelength and θ the scattering angle. At the lowest Q values, the data only contain translational diffusion contributions. In Gaussian approximation we have

$$S(Q,t)/S(Q) = e^{-(Q^2/6)\langle r_{\mathrm{c.m.}}^2(t)\rangle}, \qquad (1)$$

where $\langle r_{\mathrm{c.m.}}^2(t)\rangle$ is the time-dependent mean square center of mass displacement of the PEG-POSS nanoparticles.

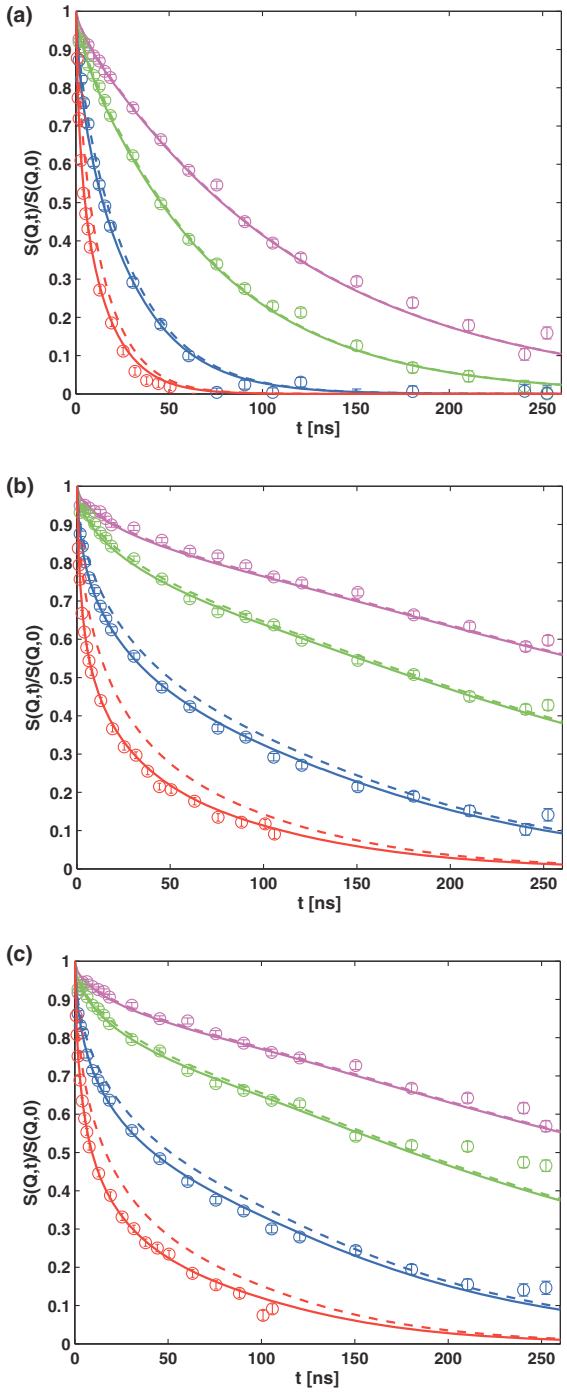

FIG. 2. Neutron spin-echo data from PEG-POSS nanoparticles in melts of *d*-PEG (a, 1.5; b, 20; c, 80 K). For 4 values of the scattering wave vector $Q = 0.07$, 0.09, 0.14 and 0.19 Å^{-1}. The dashed lines show the contribution of NP center of mass diffusion. The solid lines include also the internal dynamics of the PEG arms attached to the POSS particles (see text).

Equation (1) allows the direct determination of $\langle r_{\mathrm{c.m.}}^2(t)\rangle$ by inversion [16].

Figure 3 presents the obtained $\langle r_{\mathrm{c.m.}}^2(t)\rangle$ for the three matrices. The lower points result from the PEG-POSS diffusion within the entangled 20 and 80 K matrices.

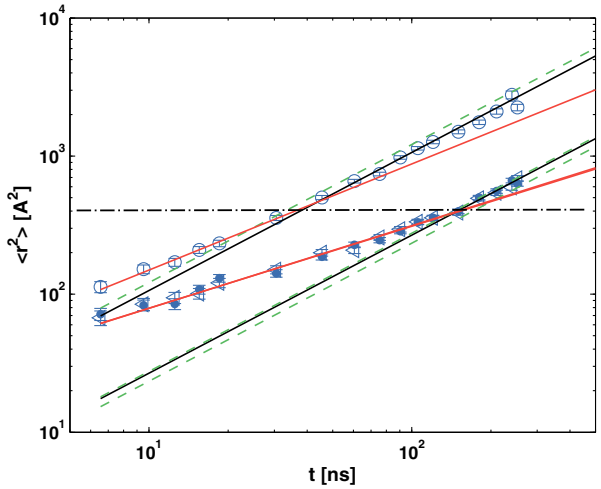

FIG. 3. MSD of the POSS particle center of mass diffusion computed from the $Q = 0.07$ Å^{-1} NSE data by inversion of Eq. (1), open circles: 1.5 K, triangles and dots: 20 and 80 K d-PEG matrix. The dashed lines indicate the MSD extrapolated from NMR results. The dash-dotted line indicates the MSD value which separates the validity regimes of sublinear diffusion (red lines) from that of normal Fickian diffusion (black lines).

At times below 150 ns, the MSD is subdiffusive following a power law $\propto t^{0.56}$. At $\tau_{\text{cross}} = 150$ ns the data indicate a crossover towards Fickian diffusion, where the MSD follows a linear time dependence. On the same samples also PFG-NMR diffusion results were obtained. The extrapolations into the nanoseconds regime are shown by the dashed lines. They agree well with the long time Fickian diffusion from the NSE data and further confirm the observed crossover.

The upper data points relate to the PEG-POSS motion within the nonentangled 1.5 K matrix. Again we see subdiffusive motion at short times, now following a power with an exponent $\alpha = 0.77$. For this sample the crossover takes place at $\tau_{\text{cross}} = 40$ ns, well in the center of the NSE time window. The dashed line again gives the extrapolation of the NMR results to the nanosecond scale. We note that (i) for the entangled matrices the PEG-POSS MSDs are independent of molecular weight (ii) for the nonentangled matrix, the diffusion is significantly faster; however, the crossover to Fickian diffusion takes place at exactly the same $\langle r^2_{\text{c.m.}}\rangle = 420$ Å^2 as in the higher M_w matrices—the crossover $\langle r^2_{\text{c.m.}}\rangle$ is indicated by the horizontal dashed line. This value virtually matches the effective radius of the particle $R = R_g\sqrt{5/3}$.

In Table I we display the quantitative results for the diffusion properties within the three matrices. Thereby $D_{\text{sub}}(t)$ results from the equation $\langle r^2_{\text{c.m.}}(t)\rangle = 6D_{\text{sub}}(t)t$. Finally, we connect the two MSD regimes by a simple crossover function $\langle r^2_{\text{c.m.}}(t)\rangle = \{[6D_{\text{sub}}(t)t]^a + [6Dt]^a\}^{1/a}$ with $a = 10$. Then by Eq. (1) we describe the diffusion contribution to the NSE spectra shown in Fig. 2 as dashed lines. As is evident, the two lowest Q values are well described solely by diffusion. At higher Q the decay of $S(Q,t)/S(Q)$ is more pronounced than what diffusion would predict.

Thus, some extra dynamics become visible. First, we consider the diffusive motion of the PEG-POSS (effective diameter $2R \simeq 41$ Å) smaller than the tube diameter $d_{\text{tube}} = 52.5$ Å of the polymer melt. According to Ref. [5], as well as to Refs. [6,17], the short-time Rouse motion within the melt is expected to be responsible for the particle dynamics. Since from various experiments [18–20] we know all microscopic parameters of the PEG melt, we may compare the experimental data quantitatively with Rubinstein's scaling predictions. Thereby we complement the scaling approach by the proper prefactors.

The basic mechanism is as follows. (i) At very short times, the NP will diffuse with the Stokes-Einstein diffusion coefficient corresponding to the monomeric PEG viscosity. (ii) As soon as the nanoparticle is covering a distance larger than a monomer or segmental size, increasingly larger chain sections will start to create friction. This results in a scale dependent viscosity, giving rise to a diffusion coefficient desreasing with time. (iii) This process saturates when the particle has covered a distance corresponding to its size. Then all Rouse modes corresponding to chain sections up to the particle size are involved and from there on the translational particle diffusion coefficient is expected to be of Fickian nature.

Let us now consider numbers. The Rouse monomeric viscosity is given by

$$\eta_{\text{mon}} = \frac{N_A\rho}{36M_0}\zeta_0 l_{st}^2 = 0.54 \text{ mPa s} \tag{2}$$

with N_A the Avogadro number, $\rho = 1040$ kg/m^3 the polymer density [21], $\zeta_0 = 0.40 \times 10^{-11}$ kg/s the monomeric friction coefficient [15,17], and, finally, $l_{\text{st}} = 5.9$ Å the matrix PEO segment length. With that we may define a short-time nanoparticle diffusion coefficient $D_0 = k_BT/(6\pi\eta_{\text{mon}}R) = 25.2$ Å^2/ns. This local diffusion coefficient will be valid until the MSD has reached the size of a monomer. Thus, we may define a basic time $6\tau_0 D_0 = l_{\text{st}}^2 \rightarrow \tau_0 = 0.23$ ns. As soon as the MSD rises beyond this value, the viscosity in the Stokes-Einstein expression has to be replaced by an effective viscosity taking into account the increasing number of segments contributing to $\eta_{\text{eff}} = \eta_{\text{mon}}\sqrt{t/\tau_0}$, [6], which for our parameters leads to an effective diffusion coefficient $D_{\text{eff}}(t) = k_BT/[6\pi\eta_{\text{eff}}(t)R] = 3.68 \times 10^{-15}$ [m^2/s$^{1/2}$]$t^{-1/2}$. D_{eff} will continue to decrease until a MSD of the particle size $R^2 = 6D_{\text{eff}}(\tau_{\text{cross}})\tau_{\text{cross}}$ is reached, thereby defining the crossover time from which the subdiffusive behavior will change into Fickian diffusion. With the present values we arrive at $\tau_{\text{cross}} = 40$ ns. The Fickian diffusion coefficient is predicted as

$$D_F = \frac{k_BTl_{\text{st}}^2}{6\pi\eta_{\text{mon}}R^3}. \tag{3}$$

TABLE I. NMR diffusometry and NSE diffusion constants and segmental friction of the PEG arms of the PEG-POSS NP.

Sample	$D_{\mathrm{NMR}}[\text{Å}^2/\mathrm{ns}]$	$D_{\mathrm{NSE}}[\text{Å}^2/\mathrm{ns}]$	$D_{\mathrm{sub}}(t)[\text{Å}^2/\mathrm{ns}]$	$\zeta_{0,\mathrm{POSS}}[10^{-11}\ \mathrm{kg/s}]$
1.5 K	2.02 ± 0.04	1.77 ± 0.04	$3.97 \times (t/\mathrm{ns})^{-0.23}$	0.61 ± 0.03
20 K	0.39 ± 0.05	0.45 ± 0.02	$3.82 \times (t/\mathrm{ns})^{-0.43}$	0.91 ± 0.04
80 K	0.46 ± 0.03	0.46 ± 0.02	$4.26 \times (t/\mathrm{ns})^{-0.46}$	1.49 ± 0.10

Inserting our parameters we get $D_F = 2$ Å^2/ns. The way our approach is constructed at τ_{cross} the center of mass MSD amounts to R^2.

We now compare the predicted quantities with the experimental results from Table I. Obviously, for the 1.5 K matrix the experimental values and the predictions are very close. The crossover is found at about 40 ns identical to the calculated 40 ns. The Fickian diffusion coefficients of 1.77 (NSE) or 2.02 Å^2/ns (NMR) are again very similar to the calculated 2 Å^2/ns. However, the scaling exponent in the subdiffusive regime is $\alpha = 0.77$, significantly larger than the predicted value of 0.5. Nevertheless, we get a nearly quantitative agreement of the measured diffusion properties for the short chain matrix, which by itself definitely follows the Rouse dynamics.

Even though qualitatively the scaling theory depicts also all features of the entangled matrices, the quantitative comparison is not favorable. First we note the excellent qualitative agreement with theory: (i) we find subdiffusivity with an exponent of $\alpha \simeq 0.56$ rather close to the predicted 0.5, (ii) the mean square displacement of the nanoparticle is independent of the matrix molecular weight in the entangled matrix, and (iii) the crossover to Fickian diffusion takes place at $\langle r^2_{\mathrm{c.m.}} \rangle = R^2$.

However, beyond the topological constraints expressed by the tube the entangled matrix seems to impose further resistance showing itself in an increase of the effective nanoparticle friction. Taking the ratio of the diffusion coefficients in the 20 or 80 K matrix with that in the 1.5 K matrix (Table I) we find an increase of the apparent friction by a factor of 4, while from the M_w dependence of the glass transition temperature at most a 10% effect is expected [18]. Thus, the microrheological viscosity on a scale inside the tube is not only determined by the Rouse friction but includes further resistance most likely relating to the topological constraints imposed by the other chains. This finding, which might be representative also for hairy nanoparticles in general, will affect the interpretation of microrheological experiments and calls for caution in identifying particle friction with Rouse friction.

From Fig. 2 it is obvious that beyond translational diffusion some additional dynamics contribute to the dynamic structure factor. These dynamics must be related to the motions of the PEG arms associated with the POSS nucleus. Because $S(Q,t)/S(Q)$ consists of a term for describing the overall center of mass diffusion multiplied with a structure factor $S(Q,t)_{\mathrm{int}}$ describing any additional internal dynamics, the latter is simply given by the division of the measured structure factor by the diffusive part [Eq. (1)]. Figure 4 displays the result for $S(Q,t)_{\mathrm{int}}/S(Q)$, describing the additional dynamics of the PEG-POSS particle in the 80 K melt. We found that a model for the Rouse dynamics of a polymer star [22,23] fits the data very well. Further details are given in the Supplemental Material [24]. The perfect agreement with the data confirms that the Rouse model for a Gaussian star polymer well describes the internal dynamics of the PEG-POSS particle. The only fitted parameter, the Rouse friction coefficient, describes the decay of the structure factor at short times. The plateau observed at longer times is solely determined by the final extension of the star taken from the SANS results. As Fig. 4 shows, the dynamic structure factor for the Gaussian star describes both features, the initial decay as well as the plateauing quite well. Analogously also the data for the 1.5 and 20 K matrices were treated. The final result, including the diffusion part, is presented by the solid lines in Figs. 2(a) and 2(b). In Table I, we present the obtained monomeric friction coefficients within the PEG-POSS shell. We note a significant increase of the friction coefficient with the increase of the host molecular weight. Thus, the matrix molecular weight affects the local viscosity of the grafted chains. The increasing friction also raises the shell viscosity [Eq. (2)]. This result has broad implications for understanding the effect of grafted

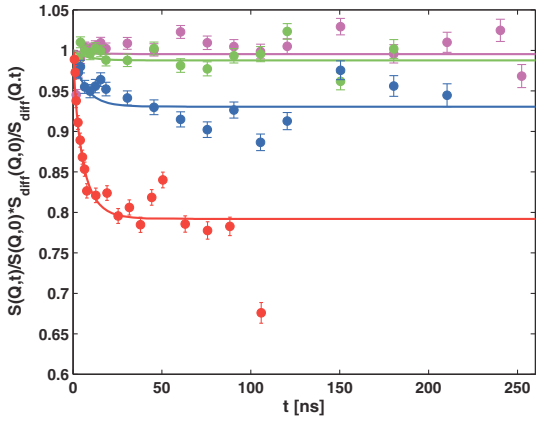

FIG. 4. NSE data from PEG-POSS in 80 K d-PEG divided by the center of mass factor in $S(Q,t)$. The lines correspond to the dynamic contribution of the star shaped arms of the PEG-POSS. The Q values are the same as in Fig. 2.

chains on their surroundings and the effect of the surroundings on the grafted chains. One immediate application relates to a matter of great technological importance, the reinforcement in polymer nanocomposites containing particles with grafted chains [27,28].

Marta Lungova thanks the EU for financial support through the ITN-214627 (DYNACOP). The support with the SANS experiments at MLZ in Garching by A. Radulescu and N. K. Szekely is acknowledged.

*Present address: Poliklinik für Präventive Zahnmedizin, Parodontologie und Kariologie Universitätsmedizin Göttingen, Georg-August-Universitt Göttingen, Germany.

[1] T. A. Waigh, Rep. Prog. Phys. **68**, 685 (2005).
[2] H. Guo, G. Bourret, M. K. Corbierre, S. Rucareanu, R. B. Lennox, K. Laaziri, L. Piche, M. Sutton, J. L. Harden, and R. L. Leheny, Phys. Rev. Lett. **102**, 075702 (2009).
[3] J. Liu, M. L. Gardel, K. Kroy, E. Frey, B. D. Hoffman, J. C. Crocker, A. R. Bausch, and D. A. Weitz, Phys. Rev. Lett. **96**, 118104 (2006).
[4] D. J. Pine, D. A. Weitz, P. M. Chaikin, and E. Herbolzheimer, Phys. Rev. Lett. **60**, 1134 (1988).
[5] F. Brochard-Wyart and P. de Gennes, Eur. Phys. J. E **1**, 93 (2000).
[6] L.-H. Cai, S. Panyukov, and M. Rubinstein, Macromolecules **44**, 7853 (2011).
[7] D. Kim, S. Srivastava, S. Narayanan, and L. A. Archer, Soft Matter **8**, 10813 (2012).
[8] H. Guo, G. Bourret, R. B. Lennox, M. Sutton, J. L. Harden, and R. L. Leheny, Phys. Rev. Lett. **109**, 055901 (2012).
[9] S. Narayanan, D. R. Lee, A. Hagman, X. Li, and J. Wang, Phys. Rev. Lett. **98**, 185506 (2007).
[10] N. Begam, S. Chandran, M. Sprung, and J. Basu, Macromolecules **48**, 6646 (2015).
[11] H. Frielinghaus, A. Feoktystov, I. Berts, and G. Mangiapia, J. Large-Scale Res. Facilities **1**, A28 (2015).
[12] M. Lungova, W. Pyckhout-Hintzen, A. Wischnewski, and D. Richter, Institut Laue Langevin (ILL); Grenoble (2013), http://doi.ill.fr/10.5291/ILL-DATA.TEST-2200.
[13] J. S. Pedersen and M. C. Gerstenberg, Macromolecules **29**, 1363 (1996).
[14] J. S. Pedersen, J. Chem. Phys. **114**, 2839 (2001).
[15] G. Smith, D. Yoon, R. Jaffe, R. Colby, R. Krishnamoorti, and L. Fetters, Macromolecules **29**, 3462 (1996).
[16] D. Richter, M. Monkenbusch, A. Arbe, and J. Colmenero, *Neutron Spin Echo in Polymer Systems*, Advances in Polymer Science, Vol. 174 (Springer, Berlin, 2005).
[17] L.-H. Cai, S. Panyukov, and M. Rubinstein, Macromolecules **48**, 847 (2015).
[18] K. Niedzwiedz, A. Wischnewski, W. Pyckhout-Hintzen, J. Allgaier, D. Richter, and A. Faraone, Macromolecules **41**, 4866 (2008).
[19] T. Glomann, G. J. Schneider, J. Allgaier, A. Radulescu, W. Lohstroh, B. Farago, and D. Richter, Phys. Rev. Lett. **110**, 178001 (2013).
[20] M. Krutyeva, A. R. Bras, W. Antonius, C. H. Hoevelmann, A. S. Poulos, J. Allgaier, A. Radulescu, P. Lindner, W. Pyckhout-Hintzen, A. Wischnewski, and D. Richter, Macromolecules **48**, 8933 (2015).
[21] J. E. Mark, *Physical Properties of Polymers Handbook* (AIP Press, New York, 2006).
[22] M. Guenza and A. Perico, Macromolecules **26**, 4196 (1993).
[23] M. Guenza, M. Mormino, and A. Perico, Macromolecules **24**, 6168 (1991).
[24] See Supplemental Material at http://link.aps.org/supplemental/10.1103/PhysRevLett.117.147803, which includes Refs. [22,23,25,26], for details on the computation of the dynamic star structure factor.
[25] J. Luettmer-Strathmann, J. Chem. Phys. **112**, 5473 (2000).
[26] D. Richter, M. Monkenbusch, A. Arbe, and J. Colmenero, *Neutron Spin Echo in Polymer Systems*, Advances in Polymer Science, Vol. 174 (Springer, Berlin, 2005).
[27] G. Huber and T. A. Vilgis, Macromolecules **35**, 9204 (2002).
[28] M. Wang and R. J. Hill, Soft Matter **5**, 3940 (2009).